First-principles calculations of the structural, electronic and optical properties of PdN and PdN_2

Mohammed S H Suleiman[1,2] **and Daniel P Joubert**[1]

School of Physics, University of the Witwatersrand, Johannesburg, South Africa
Department of Physics, Sudan University of Science and Technology, Khartoum, Sudan

E-mail: `suleiman@aims.ac.za (M Suleiman)`

Abstract. The atomic and electronic structures of PdN and PdN_2 were investigated using ab initio density-functional theory (DFT). We studied cohesive energy vs. volume data for a set of reported and hypothetical structures. Obtained data was fitted to a third-order Birch-Murnaghan equation of state (EOS) so as to identify the energetically most stable phases and to determine their equilibrium structural parameters. Electronic properties were investigated by calculating the band structure and the total and partial density of states (DOS). Some possible pressure-induced phase transitions were tested. To derive the frequency-dependent optical spectra (i.e. absorption coefficient, reflectivity, refractive index, and energy-loss), we performed GW_0 calculations within the random-phase approximation (RPA) to the dielectric tensor. Obtained results were compared with previous studies.

1. Introduction

In 2007, Crowhurst *et al.* [1] reported the synthesis of the new palladium nitride compound and argued for its PdN_2 stoichiometry and pyrite (C2) structure. However, many transition-metal nitrides are known to form more than one nitride [2], and first-principles methods are commonly employed to search for possible stable phases.

In this work, we consider PdN and PdN_2 stoichiometries in possible crystal structures. PdN is investigated in the following nine structures: NaCl (B1) structure, CsCl (B2) structure, the hexagonal structures of BN (B_k) and WC (B_h), wurtzite structure (B4), cooperite structure (B17), and the face-centered orthorhombic structure of TlF (B24); while PdN_2 is investigated in the following four structures: fluorite structure (C1), pyrite structure (C2), marcasite structure (C18), and the simple monoclinc structure of $CoSb_2$.

2. Electronic optimization details

Our electronic structure calculations were based on spin density functional theory (SDFT) [3, 4] within the projector augmented wave (PAW) method [5, 6] in which scalar kinematic relativistic effects are incorporated via mass-velocity and Darwin corrections in the construction of the pseudo-potentials, as implemented in VASP package [7, 8]. In solving Kohn-Sham (KS) equations [9]

$$\left\{ -\frac{\hbar^2}{2m_e}\nabla^2 + \int d\mathbf{r}' \frac{n(\mathbf{r}')}{|\mathbf{r}-\mathbf{r}'|} + V_{ext}(\mathbf{r}) + V_{XC}^{\sigma,\mathbf{k}}[n(\mathbf{r})] \right\} \psi_i^{\sigma,\mathbf{k}}(\mathbf{r}) = \epsilon_i^{\sigma,\mathbf{k}} \psi_i^{\sigma,\mathbf{k}}(\mathbf{r}), \tag{1}$$

the pseudo part of the KS one-electron spin orbitals $\psi_i^{\sigma,\mathbf{k}}(\mathbf{r})$ are expanded on a basis set of plane-waves (PWs) with energy cut-off $E_{cut} = 600$ eV. $\mathbf{\Gamma}$-centered Monkhorst-Pack meshes [10] were used to sample the first Brillouin zone (BZ), and the Perdew-Burke-Ernzerhof (PBE) parametrization [11] of the generalized gradient approximation (GGA) [12] was used for the exchange-correlation (XC) potentials. For static calculations of the total electronic energy and the density of states (DOS), partial occupancies were set using the tetrahedron method with Blöchl corrections, while in the geometry relaxation, the smearing method of Methfessel-Paxton (MP) was followed.

3. Equation of states and structural properties

To study the energy-volume $E(V)$ equation of state (EOS), and to determine the equilibrium parameters of each structure, we make isotropic variations of the cell volume while ions with free internal parameters were allowed to search for local minima on the Born-Oppenheimer potential hyper-surface [13], following the implemented conjugate-gradient (CG) algorithm, untill all Hellmann-Feynman force components [14] on each ion were smaller than $1 \times 10^{-2} eV/\mathring{A}$. The obtained cohesive energies E_{coh}, as a function of volume V per atom, were fitted to a Birch-Murnaghan 3rd-order EOS [15], and the equilibrium volume V_0, the equilibrium cohesive energy E_0, the equilibrium bulk modulus B_0 and its pressure derivative B_0' were determined by a least-squares method.

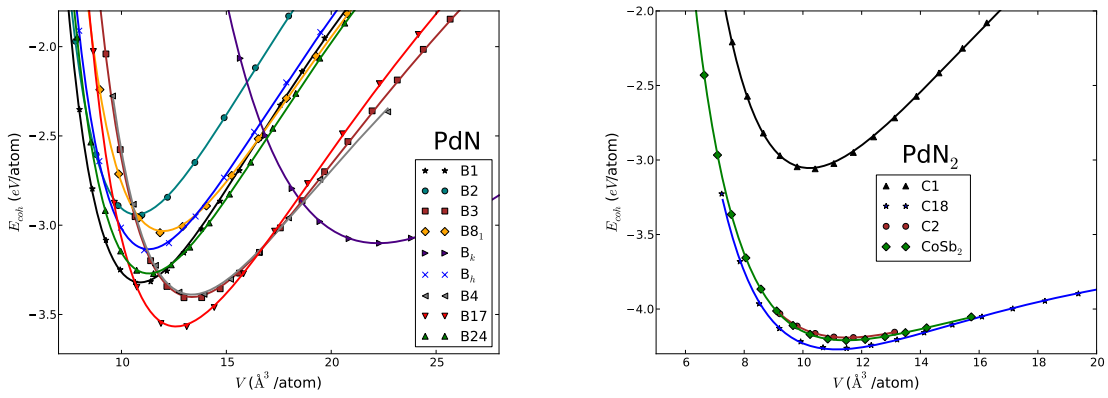

(a) (b)

Figure 1: (Color online.) Cohesive energy $E_{\rm coh}(eV/\text{atom})$ versus atomic volume V (Å^3/atom) for (a) PdN in nine different structural phases, and (b) for PdN_2 in four different structural phases.

In Fig. 1 we display the energy-volume EOS of all the studied structures, while in tabel 1, we present some of the obtained equilibrium structural parameters and compare them with some earlier theoretical calculations.

It is clear that the simple tetragonal structure of cooperite (B17) would be the energetically most stable phase of PdN (Fig. 1(a)). To the best of our knowledge, this structure has not been considered for PdN in any earlier work, though it was theoretically predicted to be the ground-state structure of platinum nitride[1] [20] in its experimentally reported stoichiometry PtN [21]. In Ref. [17] the $E(V)$ EOS for PdN in the B1, B2, B3 and B4 structures was studied. Within

[1] We also found it to be the most stable structure of CuN as well (to be reported elsewhere).

Table 1. Calculated equilibrium structural properties of some of the studied phases of PdN and PdN_2**:** Lattice constants ($a(\AA)$, $b(\AA)$, $c(\AA)$ and $\beta(^\circ)$), atomic volume $V_0(\AA^3/\text{atom})$, cohesive energy $E_{\text{coh}}(eV/\text{atom})$, bulk modulus B_0 (GPa) and its pressure derivative B_0'. The cited data are of previous DFT calculations.

Phase	a(Å)	b(Å)	c(Å)	$\beta(^\circ)$	V_0 (Å^3/atom)	$E_{\text{coh}}(eV/\text{atom})$	B_0 (GPa)	B_0'
PdN(B1)	4.444	–	–	–	10.97	3.325	207.7	4.98
	4.145 [16]	–	–	–	–	4.027 ± 0.15 [16]	–	–
	4.67 [17]	–	–	–	–	11.9 [17]	297.67 [17]	4.15 [17]
PdN(B4)	3.360	–	5.503	–	13.45	3.395	164.2	4.98
	3.37 [17]	–	5.26 [17]	–	–	11.43 [17]	171.34 [17]	4.63 [17]
PdN(B17)	3.061	–	5.389	–	12.62	3.579	190.4	4.99
PdN_2(C2)	5.169	–	–	–	11.51	4.192	69.3	5.4
	4.975 [18]	–	–	–	10.27 [18]	–	135 [18]	–
	4.843 [19]	–	–	–	18.887 [19]	–	156 [19]	9.48 [19]
PdN_2(C18)	3.173	4.164	5.082	–	11.19	4.264	76.6	6.1
	3.911 [18]	4.975 [18]	3.133 [18]	–	10.33 [18]	–	100 [18]	–
$PdN_2(CoSb_2)$	5.608	5.304	9.630	151.2	11.49	4.211	71.8	6.5
	5.071 [18]	5.005 [18]	5.071 [18]	–	10.43 [18]	–	93 [18]	–

this parameter sub-space, the relative stabilities arrived at in that work agree very well with ours. However, their obtained E_{coh} are more than twice the values we obtained, and the bulk moduli differ considerably!

In the studied parameter sub-space of PdN_2, the marcasite structure (C18) is the most energetically stable. The relative stability of C2 and $CoSb_2$ phases may be compared with Crowhurst *et al.* [1] who found PdN_2 in the baddeleyite structure (which is very close to $CoSb_2$ structure [22]) to be more stable than PdN_2(C2).

From a combined theoretical and experimental investigation, Åberg *et al.* [23] showed that for PdN_2(C2) both the electronic and the structural degrees of freedom have a strong pressure dependence. They claimed that the EOS cannot be accurately described within the GGA. Earlier calculations showed that PdN_2(C2) is very soft (see Ref. 22 in [1]). These two facts may explain the difficulty we found in relaxing this structure as well as they may explain the considerable differences found with and among the earlier reported structural properties.

4. Electronic properties

The DFT(GGA) calculated electronic band structures for PdN(B17) and PdN_2(C18) and their correponding total and partial DOS are displayed in Fig. 2 and Fig. 3, respectively. Both phases show clear metallic feature, though PdN_2(C18) has a very low TDOS around Fermi level E_F coming mainly from the d states of the Pd atoms.

5. Pressure-induced phase transitions

Enthalpy-pressure relations for PdN in some of the considered structures are displayed in Fig. 4. A point at which enthalpies $H = E_{coh}(V) + PV$ of two structures are equal defines the transition pressure P_t, where transition from the phase with higher enthalpy to the phase with lower enthalpy may occur.

Some possible transitions and the corresponding P_t's are depicted in Fig. 4. From both Fig. 1(a) and Fig. 4, it is clear that, in this parameter sub-space, B17 structure is prefered at pressures below ~ 25 GPa, while B1 structure, the most popular structure for transition-metal mono-nitrides, is favoured at higher pressures.

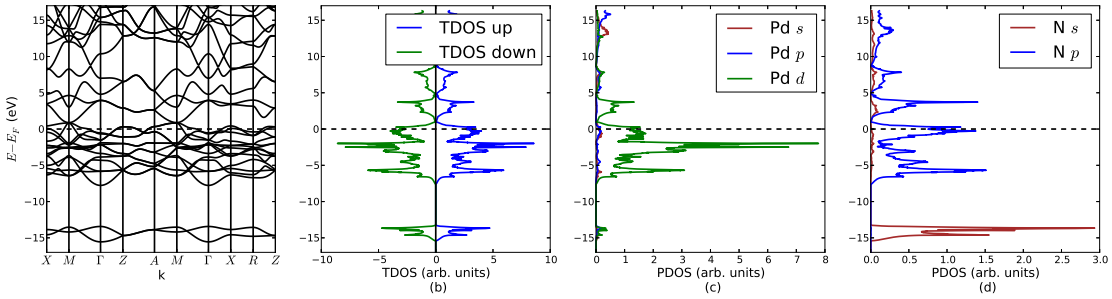

Figure 2: (Color online.) DFT calculated electronic structure for PdN in the B17 structure: **(a)** electronic band structure along the high-symmetry **k**-points, **(b)** spin-projected total density of states (TDOS); **(c)** partial density of states (PDOS) of Pd(s, p, d) orbitals in PdN; and **(d)** PDOS of N(s, p) orbitals in PdN.

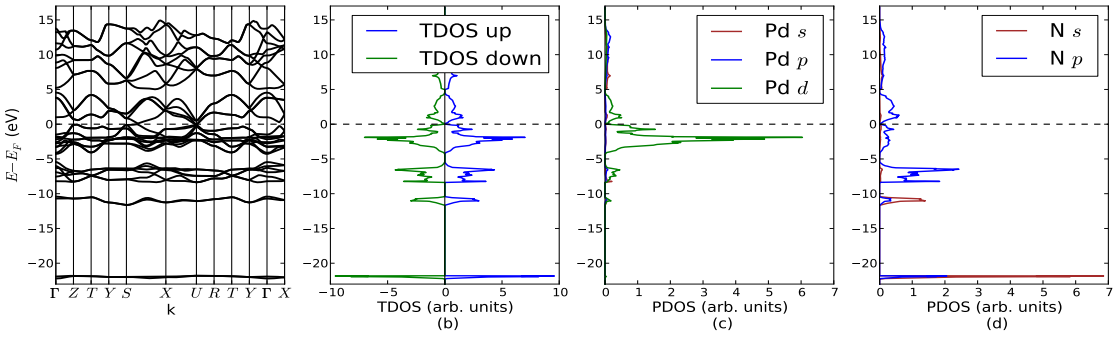

Figure 3: (Color online.) DFT calculated electronic structure for PdN_2 in the C18 structure: **(a)** electronic band structure along the high-symmetry **k**-points, **(b)** spin-projected total density of states (TDOS); **(c)** partial density of states (PDOS) of Pd(s, p, d) orbitals in PdN_2; and **(d)** PDOS of N(s, p) orbitals in PdN_2.

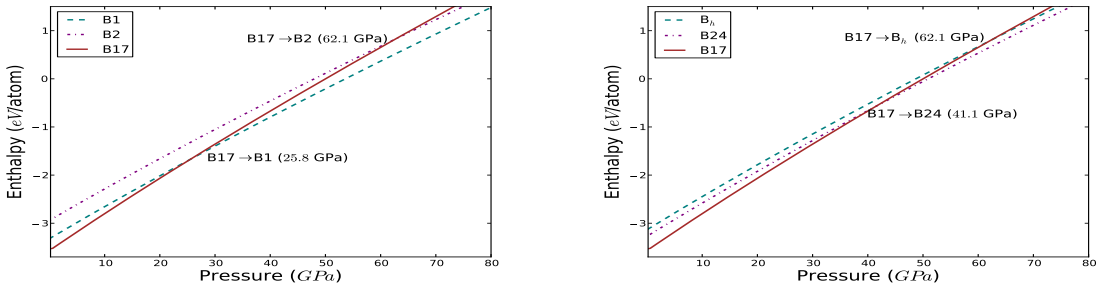

Figure 4: (Color online.) Enthalpy-pressure relations for some PdN phases in the phase transition pressure regions for the (a) B17→B1, B17→B2, (b) B17→B_h and B17→B24 phase transitions.

6. *GW* Calculations and Optical properties

In order to quantitatively improve the calculated electronic structure, and to investigate the optical spectra, we followed an alternative approach to DFT provided by many-body perturbation theory (MBPT), which leads to a system of quasi-particle (QP) equations [24]

$$\left\{ -\frac{\hbar^2}{2m}\nabla^2 + \int d\mathbf{r}' \frac{n(\mathbf{r}')}{|\mathbf{r}-\mathbf{r}'|} + V_{ext}(\mathbf{r}) \right\} \psi^{QP}_{i,\mathbf{k}}(\mathbf{r}) + \int d\mathbf{r}' \Sigma(\mathbf{r},\mathbf{r}';\epsilon^{QP}_{i,\mathbf{k}}) \psi^{QP}_{i,\mathbf{k}}(\mathbf{r}') = \epsilon^{QP}_{i,\mathbf{k}} \psi^{QP}_{i,\mathbf{k}}(\mathbf{r}). \quad (2)$$

To calculate the self-energy Σ, we followed the GW_0 self-consistent routine on the one particle's Green's function G within the random-phase approximation (RPA)[2] to the frequency-dependent dielectric tensor $\varepsilon(\omega)$. The obtained real $\varepsilon_{re}(\omega)$ and imaginary $\varepsilon_{im}(\omega)$ parts of $\varepsilon_{\mathrm{RPA}}(\omega)$ were used to derive the frequency-dependent absorption coefficient $\alpha(\omega)$, reflectivity $R(\omega)$, refractive index $n(\omega)$, and energy-loss spectrum $L(\omega)$:

$$\alpha(\omega) = \sqrt{2}\omega \left(\left[\varepsilon^2_{re}(\omega) + j\varepsilon^2_{im}(\omega) \right]^{\frac{1}{2}} - \varepsilon_{re}(\omega) \right)^{\frac{1}{2}} \quad (3)$$

$$R(\omega) = \left| \frac{\left[\varepsilon_{re}(\omega) + j\varepsilon_{im}(\omega) \right]^{\frac{1}{2}} - 1}{\left[\varepsilon_{re}(\omega) + j\varepsilon_{im}(\omega) \right]^{\frac{1}{2}} + 1} \right|^2 \quad (4)$$

$$n(\omega) = \frac{1}{\sqrt{2}} \left(\left[\varepsilon^2_{re}(\omega) + \varepsilon^2_{im}(\omega) \right]^{\frac{1}{2}} + \varepsilon_{re}(\omega) \right)^{\frac{1}{2}} \quad (5)$$

$$L(\omega) = \frac{\varepsilon_{im}(\omega)}{\varepsilon^2_{re}(\omega) + \varepsilon^2_{im}(\omega)} \quad (6)$$

Fig. 5 displays the real and the imaginary parts of $\varepsilon_{\mathrm{RPA}}(\omega)$ for PdN(B24) and the corresponding derived optical constants within the optical region. It is clear from the absorption coefficient $\alpha(\omega)$ spectrum (Fig. 5, low right) that GW_0 calculations show that B24 is a metallic phase of PdN.

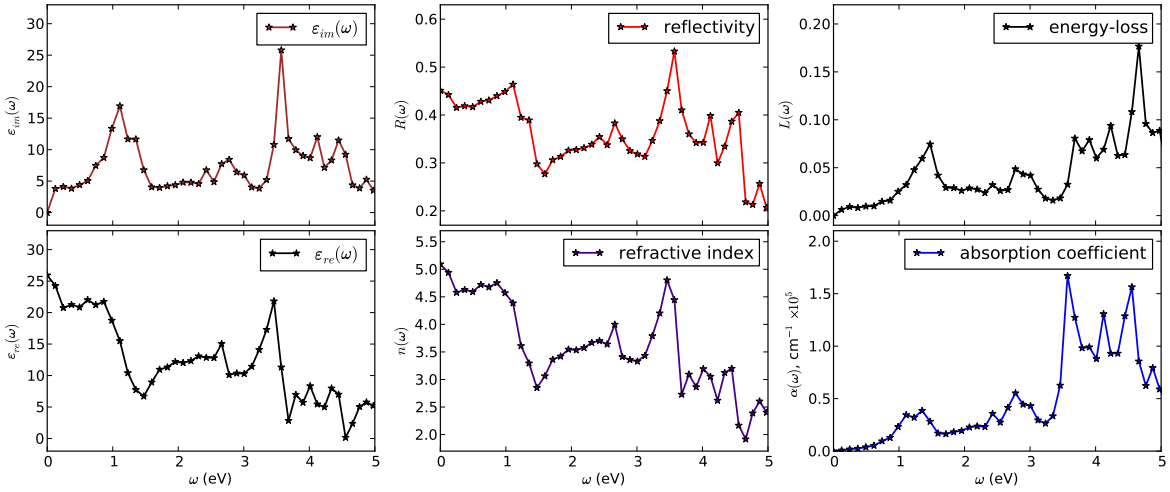

Figure 5: (Color online.) The real and the imaginary parts of the frequency-dependent dielectric function and the corresponding optical constants of PdN(B24).

[2] *c.f.* Ref.[25] and references there in

7. Conclusion

We have applied first-principles methods to investigate the structural, electronic and optical properties of some possible stoichiometries and crystal structures of palladium nitride. The considerable differences found with and among the earlier reported structural properties may invoke the need for deeper and more expensive investigation schemes such as in Ref. [23].

Acknowledgments

Suleiman would like to thank Dr. Mahlaga P. Molepo for carefully reading the manuscript and for giving valuable comments.

References

[1] Crowhurst J C, Goncharov A F, Sadigh B, Zaug J, Aberga D, Meng Y and Prakapenka V B 2008 *Journal of Materials Research* **23** 1 – 5 URL http://journals.cambridge.org/action/displayAbstract?fromPage=online&aid=7953263

[2] Wells A F 1984 *Structural Inorganic Chemistry* 5th ed (Oxford University Press)

[3] von Barth U and Hedin L 1972 *Journal of Physics C: Solid State Physics* **5** 1629–1642 URL http://iopscience.iop.org/0022-3719/5/13/012/

[4] Pant M and Rajagopal A 1972 *Solid State Communications* **10** 1157 – 1160 ISSN 0038-1098 URL http://www.sciencedirect.com/science/article/pii/0038109872909349

[5] Blöchl P E 1994 *Physical Review B* **50**(24) 17953–17979 URL http://link.aps.org/doi/10.1103/PhysRevB.50.17953

[6] Kresse G and Joubert D P 1999 *Physical Review B* **59**(3) 1758–1775 URL http://link.aps.org/doi/10.1103/PhysRevB.59.1758

[7] Kresse G and Hafner J 1993 *Physical Review B* **47**(1) 558–561 URL http://link.aps.org/doi/10.1103/PhysRevB.47.558

[8] Kresse G and Hafner J 1994 *Physical Review B* **49**(20) 14251–14269 URL http://link.aps.org/doi/10.1103/PhysRevB.49.14251

[9] Kohn W and Sham L J 1965 *Physical Review* **140**(4A) A1133–A1138 URL http://link.aps.org/doi/10.1103/PhysRev.140.A1133

[10] Monkhorst H J and Pack J D 1976 *Physical Review B* **13**(12) 5188–5192 URL http://link.aps.org/doi/10.1103/PhysRevB.13.5188

[11] Perdew J P, Burke K and Ernzerhof M 1996 *Physical Review Letters* **77**(18) 3865–3868 URL http://link.aps.org/doi/10.1103/PhysRevLett.77.3865

[12] Becke A D 1988 *Physical Review A* **38**(6) 3098–3100 URL http://link.aps.org/doi/10.1103/PhysRevA.38.3098

[13] Born M and Oppenheimer J R 1927 *Annalen der Physik* **84** 457–484

[14] Feynman R P 1939 *Physical Review* **56**(4) 340–343 URL http://link.aps.org/doi/10.1103/PhysRev.56.340

[15] Birch F 1947 *Physical Review* **71**(11) 809–824 URL http://link.aps.org/doi/10.1103/PhysRev.71.809

[16] Fernández Guillermet A, Häglund J and Grimvall G 1992 *Phys. Rev. B* **45**(20) 11557–11567 URL http://link.aps.org/doi/10.1103/PhysRevB.45.11557

[17] Deligoz E, Colakoglu K and Ciftci Y O 2010 *physica status solidi (b)* **247** 2155–2160 ISSN 1521-3951 URL http://dx.doi.org/10.1002/pssb.200945578

[18] Chen W, Tse J S and Jiang J Z 2010 *Journal of Physics: Condensed Matter* **22** 015404 URL http://stacks.iop.org/0953-8984/22/i=1/a=015404

[19] Wen-Jie Z and Yuan-Xu W 2009 *Chinese Physics B* **18** 3934 URL http://stacks.iop.org/1674-1056/18/i=9/a=053

[20] von Appen J, Lumey M W and Dronskowski R 2006 *Angewandte Chemie International Edition* **45** 4365–4368 ISSN 1521-3773 URL http://dx.doi.org/10.1002/anie.200600431

[21] Gregoryanz E, Sanloup C, Somayazulu M, Badro J, Fiquet G, kwang Mao H and Hemley R J 2004 *Nature Materials* **3** 294 – 297 URL http://www.nature.com/nmat/journal/v3/n5/full/nmat1115.html

[22] Friedrich A, Winkler B, Juarez-Arellano E A and Bayarjargal L 2011 *Materials* **4** 1648–1692 ISSN 1996-1944 URL http://www.mdpi.com/1996-1944/4/10/1648

[23] Åberg D, Erhart P, Crowhurst J, Zaug J M, Goncharov A F and Sadigh B 2010 *Phys. Rev. B* **82**(10) 104116 URL http://link.aps.org/doi/10.1103/PhysRevB.82.104116

[24] Kohanoff J 2006 *Electronic Structure Calculations for Solids and Molecules : Theory and Computational Methods* (Cambridge University Press; Cambridge)

[25] Aryasetiawan F and Gunnarsson O 1998 *Reports on Progress in Physics* **61** 237 URL http://stacks.iop.org/0034-4885/61/i=3/a=002